1 Title

- 2 Mitochondria-derived vesicles deliver antimicrobial payload to control phagosomal
- 3 bacteria

4 Authors/Affiliations

- 5 Basel H. Abuaita*, Tracey L. Schultz, and Mary X. O'Riordan*
- 6 Department of Microbiology and Immunology, University of Michigan School of
- 7 Medicine, Ann Arbor, MI 48109, USA
- 8 Author List Footnotes
- 9 Contact Info
- 10 *Correspondence: <u>oriordan@umich.edu</u>
- 11

12 Summary

13

Pathogenic bacteria taken up into the macrophage phagosome are the target of many anti-microbial effector molecules. Although mitochondria-derived antimicrobial effectors such as reactive oxygen species (mROS) are reported to aid in bacterial killing, it is unclear how these effectors reach bacteria within the phagosomal lumen. To examine the crosstalk between mitochondria and phagosomes, we monitored the production and the spatial localization of mROS during methicillin-resistant *Staphylococcus aureus* (MRSA) infection. We showed here mROS, specifically hydrogen peroxide (mH₂O₂) can

be delivered into phagosomes via infection-induced mitochondria-derived vesicles, 21 which are generated in a Parkin-dependent manner. Accumulation of mH_2O_2 in 22 23 phagosomes required TLR signaling and the mitochondrial superoxide dismutase, Sod2, which converts superoxide into mH_2O_2 . These data highlight a novel mechanism 24 by which the mitochondrial redox capacity enhances macrophage antimicrobial function 25 by delivering mitochondria-derived effector molecules into bacteria-containing 26 phagosomes. 27

28

29 Introduction

30

Reactive oxygen species (ROS) play pivotal roles in signaling and defense of biological 31 organisms. These highly reactive molecules oxidize lipids, proteins and other cellular 32 constituents, leading to a spectrum of responses ranging from altered signaling to cell 33 death. While ROS are constitutively generated and de-toxified during cellular 34 metabolism, ROS levels acutely increase during cellular stress (Holmstrom and Finkel, 35 36 2014), and can be a potent weapon in the host arsenal to control invading pathogens. In cells of the innate immune system, like macrophages, ROS are primarily generated by 37 the phagocyte NADH oxidase and mitochondrial metabolism. Upon infection, the 38 39 phagocyte oxidase multi-protein complex, also referred to as NOX2, can be recruited to phagosomal membranes to generate a burst of superoxide into the phagosome lumen 40 and Kettle, 2013). However, many bacterial 41 (Winterbourn pathogens, like 42 Mycobacterium tuberculosis, Salmonella enterica serovar Typhimurium, Coxiella burnetti, and Francisella tularensis prevent the rapid NOX2-mediated burst either by 43

avoiding complex recruitment or by utilizing detoxification mechanisms (Celli and Zahrt,
2013; Koster et al., 2017; Mertens and Samuel, 2012; Vazquez-Torres and Fang,
2001). Mitochondrial ROS (mROS) can also contribute to bacterial killing (West et al.,
2011), but how these reactive molecules reach bacteria within the macrophage
phagosome is ill-defined.

49

ROS induction can be driven by cellular stress response pathways (Bronner et al., 50 2015), like the endoplasmic reticulum unfolded protein response (UPR), which is 51 activated by the three ER sensors, PERK, ATF6 and IRE1 α (Zeeshan et al., 2016; 52 Zhang and Kaufman, 2004). Indeed, many studies support an integral role for cellular 53 stress pathways in modulating innate immune responses (Muralidharan and Mandrekar, 54 2013). We recently showed that IRE1 α is critical for stimulating macrophage anti-55 microbial function (Abuaita et al., 2015). Specifically, IRE1 α activation resulted in 56 sustained macrophage ROS production required for killing MRSA. Notably, IRE1 α 57 dependent killing was only partially NOX2-dependent, despite the well established role 58 of NOX2 in neutrophil oxidative defenses against Staphylococcus aureus (Rigby and 59 DeLeo, 2012). Since IRE1 α signaling induces mROS production (Tufanli et al., 2017), 60 we hypothesized that the mechanism by which IRE1 α activation led to MRSA killing 61 relied on mROS generation. 62

63

Here we show that infection of macrophages by MRSA stimulates IRE1 α -dependent production of mROS, specifically hydrogen peroxide mH₂O₂. Infection also triggers generation of Parkin- dependent mitochondrial-derived vesicles (MDVs), previously described as a pathway for mitochondrial quality control (Soubannier et al., 2012a).
These MDVs deliver the mitochondrial peroxide-generating enzyme, Sod2, into the
bacteria-containing phagosome, controlling bacterial burden. Our findings reveal a
mechanism by which programmed cellular stress responses repurpose a mitochondrial
quality control mechanism to enable anti-microbial defense.

- 72
- 73 **Results**
- 74

75 Induction of mROS by IRE1α promotes macrophage bactericidal function

We previously showed that MRSA infection stimulates macrophages to produce global 76 ROS via the activation of the ER stress sensor IRE1 α , which was required *in vitro* and 77 in vivo for effective MRSA killing (Abuaita et al., 2015). Although the phagocyte NADPH 78 oxidase-2 (NOX2) complex contributed somewhat to MRSA killing by macrophages, 79 IRE1 α stimulated robust macrophage bactericidal activity even in the absence of NOX2. 80 Previous reports indicated that mitochondrial ROS (mROS) enhance macrophage 81 bactericidal function (Geng et al., 2015; West et al., 2011), so we hypothesized that 82 IRE1 α -dependent antimicrobial activity might rely specifically on mROS. To test this 83 hypothesis, we assessed whether mROS was induced by macrophages in response to 84 MRSA infection. First, we validated that MitoPY1, a mitochondrially targeted probe that 85 fluoresces in response to mH₂O₂ (Dickinson and Chang, 2008; Dickinson et al., 2013), 86 was indeed mitochondrially restricted in macrophages. RAW264.7 cells were 87 transfected with mito-mCherry and loaded with MitoPY1. MitoPY1 fluorescence intensity 88 increased when macrophages were stimulated with exogenous H₂O₂, and the signal co-89

localized with mito-mCherry (Fig. 1A). We also quantified the difference in mean 90 fluorescence intensity (MFI) by flow cytometry (Fig. 1B). During MRSA infection, 91 MitoPY1 fluorescence intensity increased over time, peaking at 4h pi (Fig. 1C). To 92 determine whether IRE1 α was required for mH₂O₂ induction by MRSA infection, we 93 generated IRE1 α -deficient macrophages using CRISPR/Cas9 (Fig. 1D and S1). IRE1 α 94 deficiency suppressed the ability of macrophages to induce mH₂O₂ during MRSA 95 infection when compared to non-target control (Fig. 1E). To test the requirement for 96 mROS in killing MRSA, infected macrophages were treated with the ROS scavenger, 97 NecroX-5, which is primarily localized to mitochondria (Kim et al., 2010; Thu et al., 98 2016). Infected macrophages treated with NecroX-5 exhibited lower MitoPY1 99 fluorescence than control-treated cells (Fig. 1F), and decreased capacity to kill MRSA 100 (Fig. 1G). These data indicate that IRE1 α is critical for infection-induced mH₂O₂, and 101 102 establishes a role for mROS in macrophage bactericidal function against MRSA.

103

104 Mitochondrial peroxide accumulation in phagosomes is TLR-dependent

We reasoned that mH_2O_2 could contribute to bactericidal function indirectly by signaling 105 and/or by direct delivery to the phagosome. If direct delivery, we might expect to see 106 mH₂O₂ accumulate in the phagosome. To monitor mH₂O₂ spatial localization during 107 infection, we imaged live cells stimulated with viable MRSA, killed MRSA or latex beads. 108 109 Macrophages were pulsed with MitoPY1 and chased 4h post-phagocytosis (Fig. 2A). 110 Hydrogen peroxide increased within the mitochondrial network during infection with live or fixed MRSA, but not with beads. We also observed smaller MitoPy1⁺ puncta 111 throughout the cell. Notably, mH₂O₂ accumulated in MRSA-containing phagosomes 112

(Fig. 2A and 2B). To visualize the dynamic distribution of mH_2O_2 during infection, we 113 performed time-lapse imaging of infected macrophages pre-loaded with MitoPY1 (Movie 114 115 S1). By 10 min pi, the MitoPY1 signal within the mitochondrial network had increased. MitoPy1⁺ puncta first associated with the bacterial phagosome at approximately 50 min 116 pi, followed by accumulation of probe within the bacteria-containing phagosome (Fig. 117 2C and Movie S1). These data suggest that mitochondrially-derived hydrogen peroxide 118 accumulates within phagosomes, and reveal the possibility that mH₂O₂ may contribute 119 to macrophage bactericidal effector function through a direct delivery mechanism. 120

121

Mitochondrial ROS induction in macrophages occurs when cells internalize beads 122 conjugated to Toll-like receptor (TLR) ligands (TLR2 and TLR4), but not beads alone 123 (West et al., 2011). To test whether TLR signaling was required for mH_2O_2 generation 124 and accumulation within MRSA-containing phagosomes, we measured MitoPY1 125 126 fluorescence intensity in wild-type (WT) and TLR2/4/9-deficient bone marrow-derived macrophages (BMDMs) during MRSA infection. We observed increased overall mH_2O_2 127 128 in both WT and TLR2/4/9 deficient BMDMs during MRSA infection, indicating that 129 mH₂O₂ induction is largely independent of TLR2/4/9 signaling (Fig. S2A). However, 130 TLR2/4/9-deficient macrophages failed to kill MRSA (Fig. S2B) and MitoPY1 131 accumulation in their MRSA-containing phagosomes was decreased compared to WT 132 macrophages (Fig. 2D and 2E), indicating that TLR signaling controls mH_2O_2 delivery to 133 or accumulation within bacteria-containing phagosomes.

134

135 Bacterial infection triggers Parkin-dependent generation of mitochondrial-derived

136 vesicles

Recent studies have revealed that mitochondrial constituents can be selectively 137 transported to other intracellular compartments by small mitochondrial-derived vesicles 138 (MDVs) (McLelland et al., 2014; Soubannier et al., 2012a). MDVs form in an early 139 dynamin related protein 1 (Drp1)-independent response to increased oxidative stress, 140 and are positive for mitochondrial markers, like Tom20. MDVs may function as a quality 141 control mechanism by delivering damaged mitochondrial components to the 142 endolysosomal pathway (Sugiura et al., 2014). A subset of MDVs associate with 143 peroxisomes, and may represent a mechanism of communication between these two 144 organelles (Neuspiel et al., 2008). Since infection increases mH₂O₂, we reasoned that 145 could trigger generation of MDVs, a potential mechanism to deliver antimicrobial 146 content from the mitochondria to the phagosome. To test this hypothesis, we first 147 148 assessed whether MDVs are induced by MRSA infection. Macrophages were infected with MRSA, and subjected to immunofluorescence analysis by high-resolution confocal 149 150 microscopy using a Tom20-specific antibody. MRSA infection stimulated an increase of 151 small Tom20⁺ particles, here referred to as MDVs, compared to bead-containing macrophages (Fig. 3A and 3B, Fig. S3). The Parkinson's Disease associated protein, 152 153 Parkin, regulates biogenesis of a subset of MDVs (McLelland et al., 2014). We therefore tested the requirement for Parkin in generating infection-induced MDVs. WT and Parkin-154 deficient (Park2^{-/-}) BMDM were infected with MRSA, and accumulation of Tom20⁺ MDVs 155 visualized by confocal microscopy. MRSA-infected Park2^{-/-} BMDM had significantly 156 157 lower numbers of Tom20⁺ MDVs compared to WT BMDM (Fig. 3C and 3D).

Collectively, these results show that MRSA infection induces formation of Tom20⁺
MDVs through a Parkin-dependent mechanism.

160

161 Parkin controls mH₂O₂ accumulation in phagosomes and promotes bactericidal

162 effector function

Polymorphic alleles of Park2 can mediate susceptibility to microbial infection (Al-163 Qahtani et al., 2016; Manzanillo et al., 2013). We hypothesized that MDVs could 164 enhance macrophage bactericidal function by facilitating mH₂O₂ accumulation within 165 phagosomes. We first measured the requirement for Parkin in mH₂O₂ accumulation in 166 phagosomes. Upon infection, Parkin-deficient macrophages produced higher levels of 167 mH_2O_2 than WT macrophages, indicating that Parkin is not necessary for mH_2O_2 168 induction (Fig. 3E). Notably, despite higher overall levels of mH₂O₂, Parkin-deficient 169 macrophages displayed only minimal accumulation of MitoPY1 in phagosomes 170 171 compared to WT macrophages (Fig. 3F and 3G). To evaluate the contribution of Parkin to macrophage bactericidal capacity against MRSA, WT and Park2--- BMDM were 172 173 infected with MRSA to assess killing. Parkin-deficient macrophages were less capable 174 of killing MRSA compared to WT macrophages (Fig. 3H). Parkin can regulate mitochondria quality control by inducing mitophagy (Matsuda et al., 2010), or by 175 176 formation of MDVs (McLelland et al., 2014). To determine if the Parkin-dependent killing 177 mechanism we observed involved mitophagy, we measured macrophage bactericidal 178 function in the presence of Mdivi-1, a small molecule of Drp1, required for mitophagy (Narendra et al., 2008), but not MDV scission (Soubannier et al., 2012a). Macrophages 179 treated with Mdivi-1 killed MRSA as efficiently as DMSO-treated macrophages (Fig. 3I). 180

These data indicate that Parkin-dependent generation of MDV enables accumulation of
 bactericidal mH₂O₂ in the macrophage phagosome.

183

We then tested the role of Parkin in innate immunity against MRSA using a 184 subcutaneous infection model, where innate immune defenses are essential for 185 bacterial clearance (Tseng et al., 2011). WT and Parkin-deficient mice were inoculated 186 with 10⁷ MRSA subcutaneously into the shaved flank. Skin lesions were excised at 3 187 days pi, and bacterial burden and pro-inflammatory cytokines were measured. Lesions 188 from Parkin-deficient mice yielded higher bacterial numbers (Fig. 4A), and increased 189 levels of KC and IL-1ß compared to WT mice (Fig. 4B and 4C). These data support a 190 role for Parkin in innate immunity against MRSA infection in vivo and suggest that 191 parkin mediates macrophage bactericidal function via delivering Tom20⁺ MDV into 192 193 phagosomes.

194

Inhibition of phagosomal acidification enhances MDV-mediated bactericidal capacity

Phagosomal acidification enhances macrophage antimicrobial function by reducing intracellular replication of certain pathogens such as *M. tuberculosis* (Sullivan et al., 2012). Conversely, other intracellular bacterial pathogens, such as *Salmonella enterica* serovar Typhimurium, are killed more efficiently when cells are treated with Bafilomycin A1 (Baf A1), an inhibitor of the vacuolar ATPase that prevents acidification and phagolysosomal fusion (Rathman et al., 1996). Notably, under stimulating conditions, Tom20⁺ MDVs accumulate when cells are treated with BafA1, presumably by

preventing their resolution into the lysosomal network and subsequent degradation 204 (Soubannier et al., 2012a; Sugiura et al., 2014). Therefore, we hypothesized that 205 206 blockade of acidification and protein degradation in lysosomes with Baf A1 (Yoshimori et al., 1991) would increase MDV accumulation and thereby enhance bactericidal 207 mROS delivery into MRSA-containing phagosomes. To determine if MDV accumulation 208 209 enhanced macrophage bactericidal function, we first quantified MDV induction in infected macrophages treated with BafA1. We observed that BafA1 treatment increased 210 Tom20⁺ MDV accumulation in MRSA-infected macrophages compared to DMSO-211 treated macrophages (Fig. 5A and 5B). BafA1-treated macrophages exhibited higher 212 levels of mROS in MRSA-containing phagosomes and killed MRSA more efficiently 213 compared to DMSO-treated cells (Fig. 5C-E). To further investigate how MDVs 214 associate with MRSA-containing phagosomes, we performed transmission electron 215 microscopy (TEM) on MRSA-infected macrophages treated with or without BafA1 at 4h 216 217 pi. We could readily observe MRSA-containing phagosomes containing double membrane-bound vesicles (Fig. 5F). When cells were treated with BafA1, MRSA 218 219 phagosomes appeared more spacious and the double membrane-bound vesicles could 220 be easily observed inside the phagosome. To determine if these vesicles were derived from mitochondria, we performed immunogold labeling using anti-Tom20 antibody, 221 222 followed by TEM. Although the immunogold fixation conditions decreased definition of 223 phagosomal membranes, Tom20⁺ particles were observed in close proximity to the 224 bacterial surface within the phagosomal space (Fig. S4). Collectively, these data suggest that preventing lysosomal acidification and protein degradation increased MDV 225 accumulation and mH₂O₂ levels in the phagosome to augment MRSA killing. 226

227

228 Sod2 is required for generation of bactericidal mH₂O₂ and is delivered to bacteria-

229 containing phagosomes

Hydrogen peroxide is constitutively generated in the mitochondria from superoxide 230 produced by electron transport that is converted by the mitochondrial manganese 231 superoxide dismutase (Sod2) (Murphy, 2009). We therefore hypothesized that Sod2 232 was required for the bactericidal mH₂O₂ induced by MRSA infection. To define the 233 spatial localization of Sod2 positive compartments relative to phagosomes, we 234 performed confocal immunofluorescence microscopy on macrophages infected with 235 MRSA or beads, staining with Sod2- and Lamp1-specific antibodies (Fig. 6A). Sod2 236 localized to the mitochondrial network in macrophages (Fig. S5) and large Sod2⁺ 237 network objects were juxtaposed to both bead- and MRSA-containing phagosomes. 238 However, small Sod2⁺ vesicles were induced during MRSA infection, and were present 239 240 within MRSA-containing phagosomes. To further quantify Sod2⁺ vesicle accumulation in MRSA-containing phagosomes, we enumerated Sod2⁺ MDV located within a 1µm 241 radius around bead- and MRSA-containing phagosomes, which were delineated by 242 Lamp1⁺ staining, and found that MRSA infection increased Sod2⁺ MDV within 243 (Fig. 6B and 6C). To determine whether Sod2 was required for phagosomes 244 bactericidal activity, we stably knocked down Sod2 in RAW264.7 macrophages (Sod2 245 KD), which was confirmed by immunoblot analysis (Fig. 6D). We first tested the 246 requirement of Sod2 in hydrogen peroxide and superoxide generation during MRSA 247 infection (Fig. 6E, S6A and S6B). Compared to control cells, Sod2 KD cells failed to 248 produce hydrogen peroxide upon MRSA infection while produced higher level of 249

superoxide regardless of MRSA infection. Although Sod2 knockdown increased mitochondria superoxide production, it did not interfere with host cell death during MRSA infection (Fig. S6C). Importantly, Sod2 depletion impaired macrophage killing of MRSA compared to NT-control cells (Fig. 6F). Together, these results suggest that Sod2 enhances MRSA killing via generation of mH₂O₂, which is delivered by MDVs to bacteria-containing phagosomes.

256

257 **DISCUSSION**

258

The generation of anti-microbial reactive oxygen intermediates is an integral weapon in 259 the innate immune arsenal. We find that infection by MRSA stimulates the production of 260 mitochondrial ROS, specifically mitochondrial hydrogen peroxide. Our results identify 261 Sod2 as a key enzyme responsible for infection-induced mH₂O₂ generation. Moreover, 262 263 these studies reveal delivery of the Sod2/mH₂O₂ payload to the phagosome by mitochondria-derived vesicles as a novel mechanism for anti-microbial killing. 264 265 Stimulation of mH₂O₂-containing MDV during infection required TLR signaling and 266 employed a Parkin-dependent pathway. Taken together, our data support a model where Sod2-driven mH₂O₂ production and accumulation via MDV delivery establish a 267 268 potent killing ground for bacterial pathogens within the macrophage phagosome.

269

Generation of MDV has been described as a quality control mechanism that could transport damaged respiratory chain complexes from mitochondria to the endolysosomal compartment for degradation (Soubannier et al., 2012a). More recent

studies reveal that MDV can carry out diverse functions within the cell, and likely 273 represent multiple vesicle populations with distinct cargo related to their function. 274 275 Sugira, et al, provided evidence for MDV generation as a critical step in peroxisome biogenesis, where MDV containing the peroxisomal proteins, Pex3 and Pex14, fuse with 276 ER-derived vesicles, containing Pex16, resulting in import-competent organelles 277 (Sugiura et al., 2017). This model of peroxisome biogenesis adds a new dimension to 278 our understanding of how MDVs carry out mitochondrial communication with other 279 organelles. Our work further identifies the phagosome as a new destination for MDVs 280 that is revealed by infection. 281

282

Soubannier et al showed that different proteins are incorporated in MDVs when 283 mitochondria are stressed with different stimuli, implying the existence of mechanisms 284 to package and transport specific cargos. For instance, exogenous ROS applied to 285 286 isolated mitochondria results in MDVs enriched in the outer membrane protein, VDAC. However, when ROS is generated by isolated mitochondria via inhibition of complex III 287 288 by Antimycin A, MDVs carried complex III subunit core2 without enrichment of VDAC 289 (Soubannier et al., 2012b). A recent study showed that in response to heat shock or 290 LPS. MDVs delivered mitochondrial antigens to antigen-loading compartment 291 independently of Parkin (Matheoud et al., 2016). In contrast, when cells are treated with 292 Antimycin A to stimulate mitochondrial ROS production, MDVs are targeted to 293 lysosomes in a Parkin-dependent manner (McLelland et al., 2014). In the context of infection, our data demonstrated that MDVs are generated in a Parkin-dependent 294 manner, similar to MDVs destined for lysosomes. Moreover, we showed that infection-295

induced MDVs contain mitochondria-specific enzyme, Sod2. Collectively, our data and
others support the idea that specific stimuli define the packaging and destination of
MDV subsets.

299

In the context of the mitochondrial matrix, Sod2 cooperates with other enzymes and 300 anti-oxidant proteins to detoxify superoxide generated by oxidative 301 metabolism. Notably, dysregulation of Sod2 is associated with many human diseases, 302 some of which are associated with increased inflammation (Flynn and Melov, 2013). 303 Altering the spatial distribution of Sod2 could disrupt the coordinated ROS detoxification 304 process, resulting in increased hydrogen peroxide production without the capacity to 305 further reduce to water. Previous studies provide some evidence to support this 306 hypothesis. Overexpression of Sod2 increased the steady state of hydrogen peroxide in 307 cancer cells, and may contribute to tumor invasion and metastasis (Nelson et al., 2003; 308 309 Ranganathan et al., 2001). In contrast, decreasing Sod2 activity in Sod2-heterozygous mice led to higher production of superoxide radical when measured by aconitase 310 311 activity, which correlate with an increase in mitochondrial oxidative damage (Williams et 312 al., 1998). Consistent with these data, our results showed that decreasing macrophage 313 Sod2 leads to elevation of steady state levels of mitochondrial superoxide and decreased generation of hydrogen peroxide during MRSA infection. As a consequence, 314 Sod2-deficient macrophages (Sod2 KD) failed to kill MRSA. Although we were not able 315 316 to successfully generate live Sod2-deficient mice, studies of Sod2 knockdown in zebrafish demonstrate a protective role for Sod2 during infection by Pseudomonas 317 aeruginosa (Peterman et al., 2015). Our studies have identified MDVs as a new delivery 318

mechanism by which antimicrobial effectors can be trafficked into the macrophage phagosome. We propose that removal of a subset of Sod2 protein from the coordinated redox environment of the mitochondrial network through packaging into MDVs allows repurposing of this enzyme from detoxification to anti-microbial defense.

323

324 Acknowledgments

325 This work was supported by NIH award R21 Al101777 (M.X.O). B.H.A. was supported

by NIH T32 Al007538, T32 HLL007517 and an American Heart Association Post-

327 doctoral fellowship. We thank O'Riordan lab members for many helpful discussions. We

328 gratefully acknowledge the Center for Live Cell Imaging (CLCI), Microscopy and Image

329 Analysis Laboratory (MIL) and Cancer Center Immunology Core at the University of

330 Michigan Medical School. We thank Dr. T. Merkel (FDA) for *Tlr*2/4/9^{-/-} femurs.

331

332 Author Contributions

B.A. performed the experiments; B.A. and M.O. designed the experiments and wrote

the manuscript; T.S. assisted in experimental preparation.

335

336 **Declaration of Interests**

337 The authors declare no competing interests.

338

339 **References**

Abuaita, B.H., Burkholder, K.M., Boles, B.R., and O'Riordan, M.X. (2015). The
 Endoplasmic Reticulum Stress Sensor Inositol-Requiring Enzyme 1alpha Augments
 Bacterial Killing through Sustained Oxidant Production. mBio 6, e00705.

Al-Qahtani, A.A., Al-Anazi, M.R., Al-Zoghaibi, F.A., Abdo, A.A., Sanai, F.M., Al-Hamoudi, W.K., Alswat, K.A., Al-Ashgar, H.I., Khan, M.Q., Albenmousa, A., *et al.* (2016). PARK2 polymorphisms predict disease progression in patients infected with hepatitis C virus. Ann Hepatol *15*, 824-833.

Boles, B.R., and Horswill, A.R. (2008). Agr-mediated dispersal of Staphylococcus aureus biofilms. PLoS pathogens *4*, e1000052.

Bronner, D.N., Abuaita, B.H., Chen, X., Fitzgerald, K.A., Nunez, G., He, Y., Yin, X.M., and O'Riordan, M.X. (2015). Endoplasmic Reticulum Stress Activates the Inflammasome via NLRP3- and Caspase-2-Driven Mitochondrial Damage. Immunity *43*, 451-462.

- Celli, J., and Zahrt, T.C. (2013). Mechanisms of Francisella tularensis intracellular pathogenesis. Cold Spring Harb Perspect Med *3*, a010314.
- Dickinson, B.C., and Chang, C.J. (2008). A targetable fluorescent probe for imaging hydrogen peroxide in the mitochondria of living cells. J Am Chem Soc *130*, 9638-9639.
- Dickinson, B.C., Lin, V.S., and Chang, C.J. (2013). Preparation and use of MitoPY1 for imaging hydrogen peroxide in mitochondria of live cells. Nat Protoc *8*, 1249-1259.
- Flynn, J.M., and Melov, S. (2013). SOD2 in mitochondrial dysfunction and neurodegeneration. Free Radic Biol Med *62*, 4-12.
- Geng, J., Sun, X., Wang, P., Zhang, S., Wang, X., Wu, H., Hong, L., Xie, C., Li, X., Zhao, H., *et al.* (2015). Kinases Mst1 and Mst2 positively regulate phagocytic induction of reactive oxygen species and bactericidal activity. Nature immunology *16*, 1142-1152.
- Holmstrom, K.M., and Finkel, T. (2014). Cellular mechanisms and physiological consequences of redox-dependent signalling. Nat Rev Mol Cell Biol *15*, 411-421.
- Kim, H.J., Koo, S.Y., Ahn, B.H., Park, O., Park, D.H., Seo, D.O., Won, J.H., Yim, H.J.,
 Kwak, H.S., Park, H.S., *et al.* (2010). NecroX as a novel class of mitochondrial reactive
 oxygen species and ONOO(-) scavenger. Arch Pharm Res *33*, 1813-1823.

Koster, S., Upadhyay, S., Chandra, P., Papavinasasundaram, K., Yang, G., Hassan, A.,
Grigsby, S.J., Mittal, E., Park, H.S., Jones, V., *et al.* (2017). Mycobacterium tuberculosis
is protected from NADPH oxidase and LC3-associated phagocytosis by the LCP protein
CpsA. Proc Natl Acad Sci U S A *114*, E8711-E8720.

Kulpa, D.A., Del Cid, N., Peterson, K.A., and Collins, K.L. (2013). Adaptor protein 1 promotes cross-presentation through the same tyrosine signal in major histocompatibility complex class I as that targeted by HIV-1. J Virol *87*, 8085-8098.

Manzanillo, P.S., Ayres, J.S., Watson, R.O., Collins, A.C., Souza, G., Rae, C.S., Schneider, D.S., Nakamura, K., Shiloh, M.U., and Cox, J.S. (2013). The ubiquitin ligase parkin mediates resistance to intracellular pathogens. Nature *501*, 512-516.

Matheoud, D., Sugiura, A., Bellemare-Pelletier, A., Laplante, A., Rondeau, C., Chemali, M., Fazel, A., Bergeron, J.J., Trudeau, L.E., Burelle, Y., *et al.* (2016). Parkinson's Disease-Related Proteins PINK1 and Parkin Repress Mitochondrial Antigen Presentation. Cell *166*, 314-327.

Matsuda, N., Sato, S., Shiba, K., Okatsu, K., Saisho, K., Gautier, C.A., Sou, Y.S., Saiki, S., Kawajiri, S., Sato, F., *et al.* (2010). PINK1 stabilized by mitochondrial depolarization recruits Parkin to damaged mitochondria and activates latent Parkin for mitophagy. J Cell Biol *189*, 211-221.

McLelland, G.L., Soubannier, V., Chen, C.X., McBride, H.M., and Fon, E.A. (2014). Parkin and PINK1 function in a vesicular trafficking pathway regulating mitochondrial quality control. EMBO J *33*, 282-295.

Mertens, K., and Samuel, J.E. (2012). Defense mechanisms against oxidative stress in Coxiella burnetii: adaptation to a unique intracellular niche. Adv Exp Med Biol *984*, 39-63.

Muralidharan, S., and Mandrekar, P. (2013). Cellular stress response and innate immune signaling: integrating pathways in host defense and inflammation. Journal of leukocyte biology *94*, 1167-1184.

Murphy, M.P. (2009). How mitochondria produce reactive oxygen species. Biochem J *417*, 1-13.

Nelson, K.K., Ranganathan, A.C., Mansouri, J., Rodriguez, A.M., Providence, K.M., Rutter, J.L., Pumiglia, K., Bennett, J.A., and Melendez, J.A. (2003). Elevated sod2 activity augments matrix metalloproteinase expression: evidence for the involvement of endogenous hydrogen peroxide in regulating metastasis. Clin Cancer Res *9*, 424-432.

Neuspiel, M., Schauss, A.C., Braschi, E., Zunino, R., Rippstein, P., Rachubinski, R.A.,
Andrade-Navarro, M.A., and McBride, H.M. (2008). Cargo-selected transport from the
mitochondria to peroxisomes is mediated by vesicular carriers. Curr Biol *18*, 102-108.

Peterman, E.M., Sullivan, C., Goody, M.F., Rodriguez-Nunez, I., Yoder, J.A., and Kim,
C.H. (2015). Neutralization of mitochondrial superoxide by superoxide dismutase 2
promotes bacterial clearance and regulates phagocyte numbers in zebrafish. Infection
and immunity *83*, 430-440.

Ranganathan, A.C., Nelson, K.K., Rodriguez, A.M., Kim, K.H., Tower, G.B., Rutter, J.L.,
Brinckerhoff, C.E., Huang, T.T., Epstein, C.J., Jeffrey, J.J., *et al.* (2001). Manganese
superoxide dismutase signals matrix metalloproteinase expression via H2O2-dependent
ERK1/2 activation. The Journal of biological chemistry 276, 14264-14270.

Rathman, M., Sjaastad, M.D., and Falkow, S. (1996). Acidification of phagosomes
containing Salmonella typhimurium in murine macrophages. Infection and immunity *64*,
2765-2773.

- Rigby, K.M., and DeLeo, F.R. (2012). Neutrophils in innate host defense against Staphylococcus aureus infections. Semin Immunopathol *34*, 237-259.
- 418 Sanjana, N.E., Shalem, O., and Zhang, F. (2014). Improved vectors and genome-wide 419 libraries for CRISPR screening. Nature methods *11*, 783-784.

Soubannier, V., McLelland, G.L., Zunino, R., Braschi, E., Rippstein, P., Fon, E.A., and
McBride, H.M. (2012a). A vesicular transport pathway shuttles cargo from mitochondria
to lysosomes. Curr Biol *22*, 135-141.

- Soubannier, V., Rippstein, P., Kaufman, B.A., Shoubridge, E.A., and McBride, H.M.
 (2012b). Reconstitution of mitochondria derived vesicle formation demonstrates
 selective enrichment of oxidized cargo. PLoS One 7, e52830.
- Sugiura, A., Mattie, S., Prudent, J., and McBride, H.M. (2017). Newly born peroxisomes
 are a hybrid of mitochondrial and ER-derived pre-peroxisomes. Nature *542*, 251-254.
- 428 Sugiura, A., McLelland, G.L., Fon, E.A., and McBride, H.M. (2014). A new pathway for 429 mitochondrial quality control: mitochondrial-derived vesicles. EMBO J *33*, 2142-2156.
- Sullivan, J.T., Young, E.F., McCann, J.R., and Braunstein, M. (2012). The
 Mycobacterium tuberculosis SecA2 system subverts phagosome maturation to promote
 growth in macrophages. Infection and immunity *80*, 996-1006.
- Thu, V.T., Kim, H.K., Long le, T., Nyamaa, B., Song, I.S., Thuy, T.T., Huy, N.Q.,
 Marquez, J., Kim, S.H., Kim, N., *et al.* (2016). NecroX-5 protects mitochondrial oxidative
 phosphorylation capacity and preserves PGC1alpha expression levels during
 hypoxia/reoxygenation injury. Korean J Physiol Pharmacol *20*, 201-211.
- Tseng, C.W., Sanchez-Martinez, M., Arruda, A., and Liu, G.Y. (2011). Subcutaneous
 infection of methicillin resistant Staphylococcus aureus (MRSA). J Vis Exp.
- Tufanli, O., Telkoparan Akillilar, P., Acosta-Alvear, D., Kocaturk, B., Onat, U.I., Hamid,
 S.M., Cimen, I., Walter, P., Weber, C., and Erbay, E. (2017). Targeting IRE1 with small
 molecules counteracts progression of atherosclerosis. Proc Natl Acad Sci U S A *114*,
 E1395-E1404.
- 443 Vazquez-Torres, A., and Fang, F.C. (2001). Salmonella evasion of the NADPH 444 phagocyte oxidase. Microbes Infect *3*, 1313-1320.
- West, A.P., Brodsky, I.E., Rahner, C., Woo, D.K., Erdjument-Bromage, H., Tempst, P.,
 Walsh, M.C., Choi, Y., Shadel, G.S., and Ghosh, S. (2011). TLR signalling augments
 macrophage bactericidal activity through mitochondrial ROS. Nature *472*, 476-480.
- Williams, M.D., Van Remmen, H., Conrad, C.C., Huang, T.T., Epstein, C.J., and
 Richardson, A. (1998). Increased oxidative damage is correlated to altered
 mitochondrial function in heterozygous manganese superoxide dismutase knockout
 mice. The Journal of biological chemistry 273, 28510-28515.

452 Winterbourn, C.C., and Kettle, A.J. (2013). Redox reactions and microbial killing in the 453 neutrophil phagosome. Antioxid Redox Signal *18*, 642-660.

454 Yoshimori, T., Yamamoto, A., Moriyama, Y., Futai, M., and Tashiro, Y. (1991). 455 Bafilomycin A1, a specific inhibitor of vacuolar-type H(+)-ATPase, inhibits acidification 456 and protein degradation in lysosomes of cultured cells. The Journal of biological 457 chemistry 266, 17707-17712.

Zeeshan, H.M., Lee, G.H., Kim, H.R., and Chae, H.J. (2016). Endoplasmic Reticulum
Stress and Associated ROS. Int J Mol Sci *17*, 327.

Zhang, K., and Kaufman, R.J. (2004). Signaling the unfolded protein response from the
 endoplasmic reticulum. The Journal of biological chemistry 279, 25935-25938.

462

463 Figure Legends

464

465 Figure 1. MRSA infection stimulates bactericidal mH₂O₂ via IRE1α

- 466 (A) Representative live fluorescent images of macrophages transfected with mCherry-
- 467 Mito-7 encoded plasmid, pulsed with MitoPY1 for 1h and chased with H_2O_2 (100 μ M) or
- 468 left untreated. Images were acquired by Olympus IX-70 inverted microscope and
- analyzed by MetaMorph for Olympus imaging software.
- (B) Flow Cytometry mean fluorescent intensity (MFI) of macrophages after pulse with
- 471 MitoPY1 for 1h and chased with H_2O_2 or left untreated.
- 472 (C) Time course measurement of MFI of macrophages when pulsed with MitoPY1 and
- an infected with MRSA and monitored over time via flow cytometry.
- (D) Immunoblots of IRE1 α and GAPHD from cell lysates from NT-control and IRE1 α KO
- 475 macrophages.
- (E) MFI of IRE1 α KO macrophages and NT-control after labeling with MitoPY1 followed
- 477 by MRSA infection and analyzed after 4h.

(F) MFI of macrophages labeled with MitoPY1 for 1h and infected with MRSA for 4h in

the presence and absence of mROS scavenger NecroX-5.

(G) Percent of intracellular MRSA killing by macrophages in the presence and absence

481 of NecroX-5. Percent killing was calculated by the following formula [1 - (CFU indicated time

482 points / CFU_{1h pi})] X 100, which represents the percent difference in CFU at indicated time

483 point relative to 1h pi.

484 MFI of MitoPY1 quantification was determined by using FlowJo software, representing a 485 geometric mean. MFI of each condition was subtracted from MFI obtained from 486 unstained cells. Graphs are presented as mean of $n \ge 3$ independent experiments +/- SD.

487 pValue: * < 0.05, **< 0.01 and ***< 0.001.

488

489 Figure 2. TLR signaling controls mH₂O₂ accumulation in the bacterial phagosome

(A) Representative fluorescent microscopy images of macrophages when pulsed with
MitoPY1 (green) for 1h and chased with beads (red) or live and dead MRSA-mcherry
(red) infection for 4h. Images were acquired by an Olympus IX-70 inverted live-cell
fluorescence microscope and analyzed by MetaMorph imaging software.

(B) Quantification of mean fluorescent intensity (MFI) of MitoPY1 associated with
 macrophage phagosomes using imageJ software. Phagosomes were defined by the
 area in the cell where red fluorescent beads or MRSA are localized.

497 (C) Time lapse imaging of macrophages pulsed with MitoPY1 for 1h (green) and then
498 infected with MRSA-mCherry (red). Time clock Minutes : Seconds.

(D) Live microscopy images of wild type (WT) and TLR 2/4/9 deficient (TLR2/4/9 KO)
macrophages pulsed with MitoPY1 (green) for 1h and then infected with MRSAmCherry (red) for 4h.

502 (E) Quantification of MFI of MitoPY1 associated with phagosomes from WT and 503 TLR2/4/9 deficient macrophages using similar criteria as in panel B.

Graphs represent averages of MitoPY1 MFI from at least 305 phagosomes pooled from
at least three independent experiments. Error bars represent standard error of the mean
(SEM). pValue: * < 0.05 and **** < 0.0001.

507

508 Figure 3. Infection induced Parkin-dependent MDVs contribute to MRSA killing

509 (A) Confocal microscopy representative images of macrophages stimulated with beads 510 (red) or infected with MRSA (Red) for 4h and stained with Tom20 (green) antibody. 511 Images were acquired by Leica TCS SP8 scanning confocal microscope and 512 deconvoluted using Huygens essential software. Right panel are processed images 513 after subtraction of Tom20 positive large objects (surface area > $0.4 \mu m^2$).

(B) Quantification of Tom20 positive smaller objects (surface area < 0.4 μ m²) per macrophage when stimulated with beads or infected with MRSA. Decovoluted confocal images were processed by Huygens essential software using the following criteria; 10% threshold, 10% seed and garbage of 50. Tom20 positive objects with surface area larger than 0.4 μ m² were filtered out and the remaining objects were enumerated per cell basis. Graphs represent means of at least 107 cells pooled from three independent experiments +/- SEM. (C) Representative confocal microscopy images of WT and Parkin deficient (*Park2^{-/-}*)
 macrophages infected with MRSA for 4h. Images were processed using similar criteria
 as in panel A.

(D) Quantification of Tom20 positive smaller objects (surface area < $0.4 \ \mu m^2$) from WT and Parkin deficient macrophages infected with MRSA. Confocal microscopy images processed as in panel B and presented as mean +/- SEM from at least 135 cells pooled from three independent experiments.

(E) Flow cytometry mean fluorescence intensity (MFI) of WT and Parkin deficient macrophages when pulsed with MitoPY1 for 1h and infected with MRSA for 4h. Data represented as geometric mean of $n \ge 3$ independent experiments +/- SD.

(F) Representative live fluorescence wide-filed microscopy images of WT and Parkin
 deficient macrophages pulsed with MitoPY1 (green) for 1h and infected with MRSA mCherry (red). Images were acquired at 4h pi and processed by MetaMorph software.

(G) Ratiometric measurement of MitoPY1 fluorescent intensity of phagosome relative to
total cellular fluorescent intensity (MFI-phagosome/MFI-cell). Phagosomes were defined
by the area of the cell where the red fluorescent MRSA-mCherry are located.

(H) Percent of MRSA intracellular killing by WT and Parkin deficient macrophages was quantified by the following formula [1 - (CFU indicated time points / CFU_{1h pi})] X 100, which represent the percent difference in CFU obtained at indicated time point relative to 1h pi. Data are presented as mean of n≥3 independent experiments +/- SD. (I) Percent of MRSA intracellular killing by RAW264.7 macrophages when treated with control DMSO or Dynamin-related protein 1 (Drp1) selective inhibitor (Mdivi-1, 25 µM).

543 pValue: * < 0.05, **< 0.01, ***< 0.001 and ****< 0.0001.

544

Figure 4. Parkin is essential for immunity during MRSA subcutaneous infection 545 (A) Bacterial burden in skin abscesses from male and female wild-type (WT) and Parkin 546 deficient C57BL/6 mice (*Park2^{-/-}*) infected subcutaneously with 10⁷ CFU of MRSA for 3 547 days. Horizontal lines represent the mean. Data are pooled from two independent 548 experiments. 549 (B-C) KC or IL1β cytokine levels in skin abscess homogenate of WT and *Park2^{-/-}* mice. 550 Cytokine levels were quantified by ELISA. Graph bars represent mean of n=13 WT and 551 12 Park2^{-/-} mice pooled from 2 independent experiments. Error bars represent standard 552 error of the mean (SEM). 553 pValue: * < 0.05, ** < 0.01 and **** < 0.0001. 554 555 Figure 5. Blocked of phagolysosome fusion enhances MDV mediated mH₂O₂ 556 killing 557 558 (A) Processed confocal microscopy representative images of RAW264.7 macrophages infected with MRSA-mCherry (red) for 4h and stained for Tom20 (green). Images were 559 acquired by Leica TCS SP8 confocal scanning microscope and deconvoluted using 560 Huygens essential software. Images were processed using the following setting; 561 Threshold: 10%, Seed: 10% and Garbage: 50. Tom20 positive large objects (surface 562 area > 0.4 μ m²) were subtracted from the original images to define Tom20 positive 563 small objects. 564

(B) Quantification of Tom20 positive small objects (MDVs) per macrophage during
MRSA-mCherry infection in the presence and absence of Bafilomycin A1. See detail in
figure 3A. Data are presented as mean of at least 110 phagosomes from each condition
pooled form three independent experiments +/- SEM.

(C) Representative live wide-field microscopy images of RAW264.7 macrophages
 pulsed with MitoPY1 (green) and chased 4h post MRSA-mCherry (red) infection in the
 presence of Bafilomycin A1 (Baf A1, 100 nM) or controlled solvent (DMSO).

572 (D) Mean fluorescent intensity (MFI) of MRSA-containing phagosomes when 573 macrophages were being pulsed with MitoPY1 (green) and chased 4h post MRSA-574 mCherry (red) in the presence and absence of Bafilomycin A1 (Baf A1, 100 nM). Data 575 represent mean of at least 321 phagosomes of each condition pooled from three 576 independent experiments +/- SEM.

(E) Percent of MRSA intracellular killing by RAW264.7 macrophages treated with Bafilomycin A1 (Baf A1, 100 nM) or control solvent (DMSO). Percent killing was quantified by the following formula [1 - (CFU indicated time points / CFU_{1h pi})] X 100, which represent the percent difference in CFU obtained at indicated time point relative to 1h pi. Graph bars represent mean of n≥3 independent experiments +/- SD.

(F) Transmission electron microscope images of macrophage MRSA-containing phagosomes. Macrophages are infected with MRSA for 4h in the presence and absence of Bafilomycin A1 (Baf A1, 100 nM). Images were acquired by using JEOL JEM-1400 Plus transmission electron microscope. Arrows indicate vesicles that are localized inside the phagosomes. 587 pValue: ** < 0.01 and **** < 0.0001.

588

589 Figure 6. Sod2 is the mitochondria payload delivered to phagosome to promote 590 mH₂O₂ killing

(A) Representative confocal microscopy images of RAW264.7 macrophages infected
with MRSA (blue) or stimulated with bead (blue) for 4h and stained for Lamp1 (red) and
Sod2 (green). Images were acquired using Leica TCS SP8 confocal scanning
microscope and deconvoluted using Huygens essential software.

(B) Confocal microscopy images of a magnified area of macrophages where bead or MRSA-containing phagosome is localized. Images in the right panel are the resulted images after subtracting large Sod2 positive objects (surface area > $0.4 \ \mu m^2$) from left panel images.

599 (C) Quantification of Sod2 positive small objects (surface area < 0.4 μ m²) of 2 μ m² area 600 of the cell where beads or MRSA are localized. Large Sod2 positive objects were 601 filtered out of the deconvoluted images and the number of remained Sod2 positive 602 objects were enumerated per 2 μ m² areas of the cell where phagsosomes were 603 localized. Data represent mean of at least 60 phagosomes from three independent 604 experiments.

(D) Immunoblots of cell lysate from RAW264.7 macrophages stably transduced with
lentivirus-encoded shRNA for non-target (NT-Control) or Sod2 (Sod2 KD), probed with
an anti-Sod2 antibody or anti-Actin antibody as a loading control.

(E) Mean fluorescent intensity (MFI) of shRNA stably knockdown Sod2 (Sod2 KD) or
 non-target (NT-Control) macrophages after pulsed with MitoPY1 and chased 4h post
 MRSA infection. Samples were acquired by flow cytometry and analyzed by FlowJo
 software. MFI represent geometric mean of of n≥3 independent experiments +/- SD.

612 (F) Intracellular MRSA killing by Sod2 knockdown (Sod2 KD) and non-target (NT-

613 Control) macrophages was quantified by using the following formula [1 - (CFU indicated time

- 614 points / CFU_{1h pi})] and expressed as percentage. Graph bars represent mean of percent
- killing of $n \ge 3$ independent experiments +/- SD.
- 616 pValue: * < 0.05, *** < 0.001 and **** < 0.0001.
- 617

618 STAR Methods

619

620 CONTACT FOR REAGENT AND RESOURCE SHARING

Reagents and resources can be obtained by directing requests to the Lead Contact,

622 Mary O'Riordan (oriordan@umich.edu)

623

624 EXPERIMENTAL MODEL AND SUBJECT DETAILS

- 625
- 626 **Mice**

627 Wild-type C57BL/6 and Park2^{-/-} are purchased from the Jackson Laboratory. Tlr2/4/9^{-/-}

have been described previously (Abuaita et al. 2015). All mice were maintained

- according to an approved protocol in the Unit for Laboratory Animal Medicine (ULAM)
- 630 facilities at the University of Michigan Medical School.

631

632 **Cells**

633 Primary bone marrow derived macrophages (BMDMs) were prepared by flushing mouse femurs in DMEM supplemented with 100 units/ml of Pen/Strep. Cells were 634 differentiated by incubation in BMDM medium (50% DMEM, 2 mM L-glutamine, 1 mM 635 sodium pyruvate, 30% L929-conditioned medium, 20% heat-inactivated fetal bovine 636 serum (FBS), 55 µM 2-mercaptoethanol, and Pen/Strep). L-929 and HEK 293T cells 637 were cultured in MEM supplemented with 2 mM L-glutamine, 1 mM sodium pyruvate, 638 1mM Non-essential amino acid (NEAA), 10 mM HEPES, and 10% heat-inactivated 639 FBS). RAW 264.7 cells were cultured in RPMI 1640 containing 2 mM L-glutamine and 640 10% heat-inactivated FBS. All cells were incubated at 37°C in 5% CO₂. 641

642

643 Bacterial infections

644 USA300 LAC, a community associated methicillin-resistant Staphylococcus aureus strain (MRSA) and its isogenic strain harboring pSarA-mCherry plasmid (MRSA-645 mCherry) (Boles and Horswill, 2008), were maintained at -80°C in LB medium 646 647 containing 20% glycerol. All strains were cultured in tryptic soy agar (TSA, Becton Dickinson), and selected colonies were grown overnight at 37°C with shaking (240 rpm) 648 649 in liquid tryptic soy broth. Bacteria were pelleted, washed and re-suspended in PBS. 650 The bacterial inoculum was estimated based on OD_{600} , and verified by plating serial 651 dilutions on TSA plates to determine colony forming units (CFU). Macrophages were infected at a multiplicity of infection (MOI) of 20 in culture medium without antibiotic for 652 45 minutes. Infected macrophages were washed three times with PBS and incubated in 653

654	medium containing 100 μ g/ml of gentamicin to kill extracellular bacteria for 15 minutes.
655	Media was exchanged with media containing 50 $\mu\text{g/mI}$ of gentamicin for the remaining
656	time of the experiments.
657	
658	METHOD DETAILS
659	
660	Macrophage bactericidal activity
661	Macrophages were seeded in a 24-well tissue culture treated plate at a density of 1.5 X

10⁵ cell/well. The next day, macrophages were infected with MRSA (MOI of 20). The 662 number of intracellular bacteria was determined by washing infected macrophages with 663 PBS, lysing with 0.1% NP-40, and enumerating bacterial CFUs via serial dilution on 664 agar plates. The percentage of killed MRSA was calculated by the following formula [1 -665 (CFU indicated time points / CFU_{1h pi})] X 100, which represents the percent difference between 666 667 CFU at indicated time points relative to 1h pi. Where indicated, macrophages were preincubated with NecroX-5 (10 µM), Bafilomycin A1 (100 nM) or Mdivi-1 (25 µM) for 30 668 minutes before infection, and all inhibitors were maintained throughout the experiment. 669

670

671 Mouse infection

Subcutaneous MRSA infection was performed as previously described (Tseng et al., 2011). Male and Female C57BL/6 mice and $Park2^{-/-}$ were shaved on the right flank. Mice were inoculated with 10⁷ bacteria in 100 µl of PBS subcutaneously on the shaved area of the skin using a 27 gauge needle. Mice were sacrificed on day 3 post-infection and skin abscesses were excised, weighed and homogenized in PBS. Total CFU per mouse abscess were enumerated by serial dilution and plating on TSA agar. Total CFU
was converted to CFU/mg of tissue weight. Cytokines were quantified by ELISA at the
University of Michigan ELISA core and converted to pg/mg of tissue weight.

680

681 Cellular mROS measurement

Macrophages were plated in 60 mm non-treated dishes and treated with 10 µM MitoPY1 682 (TOCRIS) or 10 µM MitoSOX (Life Technology) for 1 hour. Macrophages were washed 683 three times with media and only when indicated, macrophages were treated for 30 684 minutes with NecroX-5 (10 µM) or control solvent prior to infection with MRSA (MOI of 685 20). For positive controls, macrophages were treated with 100 µM hydrogen peroxide 686 or 10 µM Antimycin A for 1 hour to induce the oxidation of MitoPY1 or MitoSOX, 687 respectively. Macrophages were subjected to flow cytometry and data were analyzed 688 689 with FlowJo software. The mean fluorescence intensity for each condition was determined as the geometric mean. 690

691

692 Phagosomal mROS measurement

Macrophages were plated in 35 mm glass bottom dishes (MatTek). The next day, macrophages were treated with MitoPY1 (10 μM) for 1 hour, washed three times with media and stimulated with inert red fluorescent beads or infected with live or dead (inactivated by paraformaldehyde) red fluorescent MRSA harboring p*SarA*-mCherry (MOI of 20). Macrophages were imaged in Ringer buffer (155 mM NaCl, 5 mM KCl, 1 mM MgCl2.6H2O, 2 mM NaH2PO4.H2O, 10 mM HEPES, and 10 mM Glucose) with an Olympus IX70 inverted live-cell fluorescence microscope. Fluorescence images were

further processed by MetaMorph imaging software. For quantification of mROS 700 association with phagosomes, the mean fluorescence intensity of MitoPY1 at the 701 702 phagosome area was measured by ImageJ. Phagosomal regions in the cell images were defined by the location of red fluorescent beads or bacteria. For BMDM 703 experiments, a ratiometric mean fluorescence intensity of the phagosomal area over the 704 705 mean fluorescence intensity of the cell was calculated. This was done because Park2 deficient macrophages have higher global MitoPY1 fluorescence intensity when 706 compared to WT macrophages prior to infection. 707

708

709 Confocal microscopy

Macrophages were seeded onto microscope cover glass and infected with MRSA (MOI 710 of 20) or stimulated with fluorescent beads. Cells were fixed at 4h pi with 3.7% 711 paraformaldehyde at room temperature for 20 minutes and permeabilized with PBS 712 713 contain 0.1% Triton X-100 for 15 minutes. MRSA were stained using chicken antiprotein A antibody conjugated to biotin (Abcam ab18598) in staining buffer (PBS, 0.1% 714 715 Triton X-100, 5% BSA, and 10% normal goat serum). Host proteins were stained using 716 mouse anti-Sod2 (Abcam ab110300, clone 9E2BD2), Rat-anti-Lamp1 (DSHB, clone 1D4B), and anti-Tom20 (Santa cruz, FL145). Secondary antibodies (goat anti-mouse 717 718 (Alexa-488), goat anti-Rat (Alexa-594) and Streptavidin (Alexa-405) were used 719 according to manufacturer's procedure. Cover glasses were mounted on microscope 720 slides using Prolong Diamond (Life Technology). Cells were imaged using a Leica TCS SP8 confocal microscope and deconvoluted using Huygens essential software by 721 scientific volume imaging using the following criteria; Threshold (10%), Seed (10%) and 722

Garbage Volume (50). To define MDVs, large objects (surface area larger than 0.4 μ m²) were filtered out from the mitochondrial fluorescence labeled channel and the number of remaining objects per cell were recorded.

726

727 Transmission electron microscopy

728 Macrophages were infected with MRSA (MOI of 20) in the presence of Bafilomycin A1 (100 nM) or control DMSO. Infected macrophages were fixed at 4h pi with 2.5% 729 glutaraldehyde for at least 1h at room temperature, then overnight at 4°C. For immuno-730 gold staining, infected macrophages were stained for Tom20 prior to fixation with 731 glutaraldehyde according to manufacturer's procedure (AURION). Briefly, cells were 732 fixed with 3.7% paraformaldehyde at room temperature for 20 minutes and 733 permeabilized with Sorenson's buffer containing 0.1% Triton X-100 for 15 minutes. Cells 734 735 were blocked with the AURION blocking solution (AURION-BSA-c) and stained using primary anti-Tom20 antibody (Santa Cruz, FL145) and secondary goat anti-rabbit ultra-736 small gold antibody (AURION). Silver stain enhancement was carried out by using the 737 AURION R-GENT SE-EM according to reagent protocol (AURION). Glutaraldehyde 738 fixed samples were washed with Sorenson's buffer 3-times before post-fixing in 2% 739 osmium tetroxide in Sorenson's buffer for 1h at room temperature. Samples were 740 washed again 3-times with Sorenson's buffer, then dehydrated through ascending 741 concentrations of ethanol, treated with propylene oxide, and embedded in EMbed 812 742 743 epoxy resin. Semi-thin sections were stained with toluidine blue for tissue identification. Selected regions of interest were ultra-thin sectioned to 70 nm and post stained with 744

uranyl acetate and Reynolds lead citrate. Sections were examined using a JEOL JEM1400 Plus transmission electron microscope (TEM) at 80 kV.

747

Generation of RAW264.7 Δ **Ire1**- α and **RAW264.7** shRNA stable knockdown cells

749 The generation of lentivirus for CRISPR-Cas9 knockout and shRNA knockdown was 750 done by using HEK293T packaging cells, which were grown in DMEM with 10% FBS. The virus particles were produced by transfecting the cells with the TRC shRNA 751 encoded plasmid (pLKO.1) or guided RNA (gRNA) encoded plasmid (lentiCRISPRv2) 752 753 along with the packaging plasmids (pHCMV-G, and pHCMV-HIV-1) (Kulpa et al., 2013) using FUGENE-HD transfection reagent (Promega). Media was changed after 24h and 754 virus particles were collected after 72h post-transfection. A total of 2 ml of medium 755 containing virus were concentrated ten-fold by ultracentrifugation at 24,000 rpm for 2h 756 757 at 4°C and used to transduce RAW264.7 cells. Transduced cells were selected with puromycin (3 µg/ml). The mouse Sod2 specific shRNA plasmid with the sense 758 sequence of (GCTTACTACCTTCAGTATAAA) and the non-target control shRNA 759 plasmid were purchased from Sigma-Aldrich. The efficiency of knockdown was 760 monitored by immunoblot analysis using anti-Sod2 antibody (Santa Cruz). Anti-Actin 761 antibody was used as a loading control (Fisher Scientific). The mouse IRE1- α specific 762 aRNA sequence of (CTTGTTGTTGTCTCGACCC) and the non-target gRNA control 763 764 sequence of (TCCTGCGCGATGACCGTCGG) were cloned into lentiCRISPRv2 according to the Feng Zhang lab protocol (Sanjana et al., 2014). Single clones of 765 RAW264.7 Δ Ire1- α were isolated and confirmed by the absence of IRE1- α protein by 766 immunoblot using anti-IRE1- α antibody (clone 14C10, Cell Signaling). Anti-GAPDH 767

antibody was used as a loading control (Santa Cruz). RAW264.7 Δ *Ire1-\alpha* clone was also confirmed by absence of its endonuclease activity when cells were treated with endoplasmic reticulum stress inducer Thapsigargin (5 μ M) by *xbp1* splicing assay (Figure S1) as previously described (Abuaita et al., 2015).

772

773 Cell death assay

Cell death was measured by flow cytometry using SYTOX green dead cell stain according to manufacturer's protocol (Life Technology). Briefly, macrophages were incubated with SYTOX green dead cell stain (30 nM) in HBSS for 20 minutes at room temperature prior to flow cytometry analysis using 488 excitation and 530/30 emission. Digitonin (0.01%, Sigma Aldrich) was used as a positive control to permeabilize the plasma membrane. The percent of SYTOX positive cells was determined by gating against mock unstained cells.

781

782 QUANTIFICATION AND STATISTICAL ANALYSIS

Data were analyzed using Excel 2016 and Student's unpaired two-tailed t-test was applied. The mean of at least three independent experiments was presented with error bars showing standard deviation (SD) or standard error of the mean (SEM), which is indicated in figure legends. *P* values of less than 0.05 were considered significant and designated by: *P < 0.05, **P < 0.01, ***P < 0.001 and ****P < 0.0001. All statistically significant comparisons within experimental groups are marked.

789

790 DATA AND SOFTWARE AVAILABILITY

- RAW data are available upon request, which should be directed to the Lead Contact.
- There was no proprietary software used in this study.

793

794 ADDITIONAL RESOURCES

- mCherry-Mito-7 plasmid was used under material transfer agreement (MTA).
- 796

797 Supplemental Information

798

Figure S1. IRE1α endonuclease activity is absent in RAW264.7ΔIRE1α macrophage cell line in response to ER Stressor, Thapsigargin

RT-PCR analysis of Xbp1 mRNA splicing in single clone of RAW 264.7 macrophages 801 stably transduced with IRE1 α specific guided RNA (gRNA) or non-target (NT-control). 802 Macrophages were treated with 5 μ M thapsigargin (TG) to induce IRE1 α endonuclease 803 804 activity or control DMSO. RT-PCR products were digested with Pstl endonuclease. Because unspliced Xbp1 mRNA contains a Pstl site within the 26 spliced region, the 805 digested RT-PCR products yield two smaller fragments representing the unspliced (U) 806 Xbp1 and one larger fragment representing the spliced (S) Xbp1. RT-PCR image is 807 representative of n≥3 independent experiments. 808

809

Figure S2. TLR2/4/9 signaling is dispensable for MRSA-induced mH₂O₂ but is
 essential for macrophage bactericidal activity

(A) Mean fluorescent intensity (MFI) of wild-type (WT) and *Tlr2/4/9* triple knockout
(TLR2/4/9 KO) macrophages that were loaded with MitoPY1 and infected with MRSA.
Macrophages were subjected to flow cytometry at 4h pi and collected data were
analyzed by FlowJo software for geometric mean.

(B) Percent of MRSA intracellular killing by WT and TLR2/4/9 KO macrophages.
Macrophage killing efficiency was calculated by using the following formula [1 - (CFU indicated time points / CFU_{1h pi})] X 100, which represent the percent difference in CFU obtained at indicated time point relative to 1h pi. Data are expressed as percentage.

Graph bars represent mean of of n≥3 independent experiments +/- SD. pValue: ** <
0.01 and **** < 0.0001.

822

Figure S3. Tom20 positive MDVs are defined by small objects that are stained with Tom20

(A) Representative confocal images of MRSA infected and beads internalized macrophages that stained for Tom20. Images were acquired by Leica TCS SP8 confocal scanning microscope and deconvoluted using Huygens essential software. Images were processed using the following setting; threshold: 10%, Seed: 10% and Garbage: 50. Right panel, Tom20 positive large objects (surface area > $0.4 \mu m^2$) were subtracted from left panel Images.

(B) Quantification the number of Tom20 positive objects per beads internalized or
 MRSA infected macrophage that fall into indicated range of surface size bins.

⁸³³ Discontinuous line was drawn to point out the surface area size bin smaller than 0.4 ⁸³⁴ μ m², which was chosen to quantify Tom20 small objects (MDVs).

835

836 Figure S4. Tom20 positive vesicles are localized in the lumen of MRSA 837 phagosomes

Transmission electron microscopy representative mages of MRSA infected macrophages when treated with Bafilomycin A1 (Baf A1, 100 nM) or control DMSO. Tom20 was stained with immune-gold particles followed by silver enhancement. Left panel; images showing whole cell, middle panel; magnified images showing mitochondria, right panel; images showing MRSA phagosome. Arrows were drawn to indicate Tom20 positive gold particles present in MRSA phagosome lumen.

844

Figure S5. Macrophage Sod2 is localized with Tom20

Representative confocal microscopy images of RAW264.7 macrophages were stained with Sod2 and Tom20. Images were acquired with Leica TCS SP8 confocal scanning microscope and deconvoluted using Huygens essential software. Pearson Correlation Coefficient (PCC) was determine on the deconvoluted images using Huygens essential software and presented as mean of at least 230 cells +/- SD pooled from three different experiments.

852

Figure S6. Knockdown macrophage Sod2 increases mitochondria superoxide production without interfering with host cell death during MRSA infection

(A) Representative histogram plots are shown when macrophages were pulsed with MitoSOX for 1h and chased 4h after stimulated with Antamycin A (10 μ M), infected with MRSA at MOI of 20 or left untreated (Mock). Percent of MitoSOX positive cells was determined by gating against unstained cells. Percent of MitoSOX high cells was determined by gating against the MitoSOX first peak.

(B) Quantification of the percentage MitoSOX high from panal A. Data represent the
 percentage of cells with MitoSOX high relative to total MitoSOX positive cells.

(C) Percent of live macrophages was determined by Sytox green dead cell staining. NTcontrol and Sod2 KD macrophages were infected with MRSA for 4h (MOI of 20), treated
with 0.01% Digitonin (Digitonin) to induce cell death or left untreated (Mock). Cells were
stained with 30 nM of Sytox green in HBSS buffer and subjected to flow cytometry. Data
are analyzed by FlowJo software. Percent of Sytox green positive cells were determined
by gating against live cell peak.

Graph bars represent mean of n \geq 3 independent experiments +/- SD. pValue: * < 0.05 and ** < 0.01.

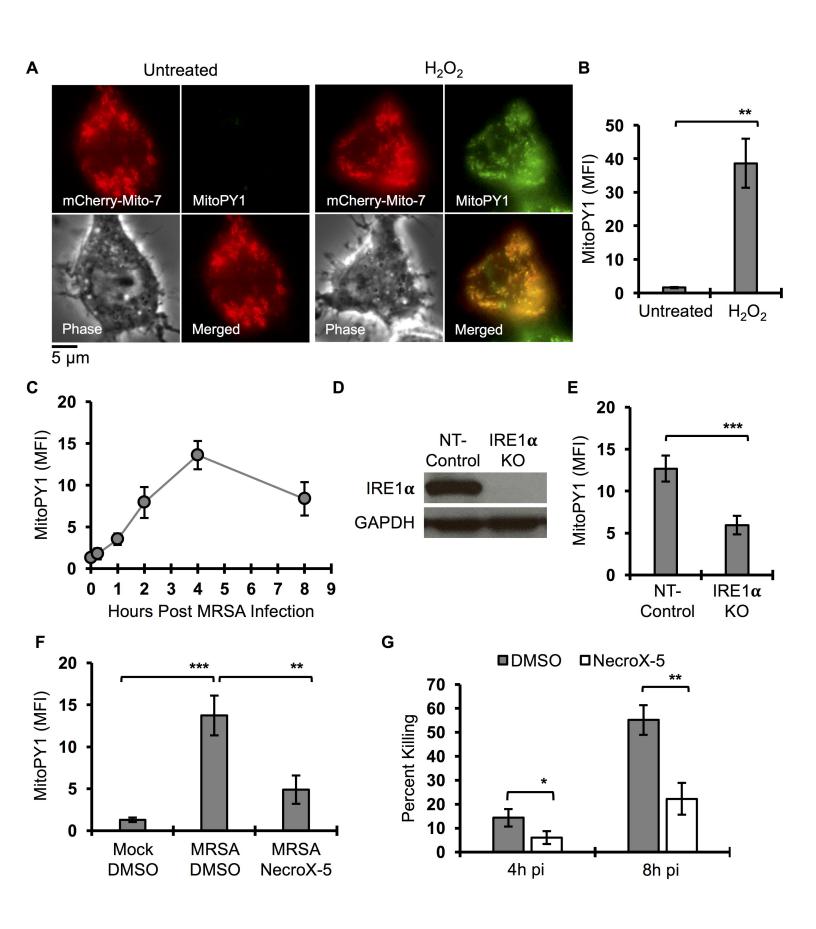
870

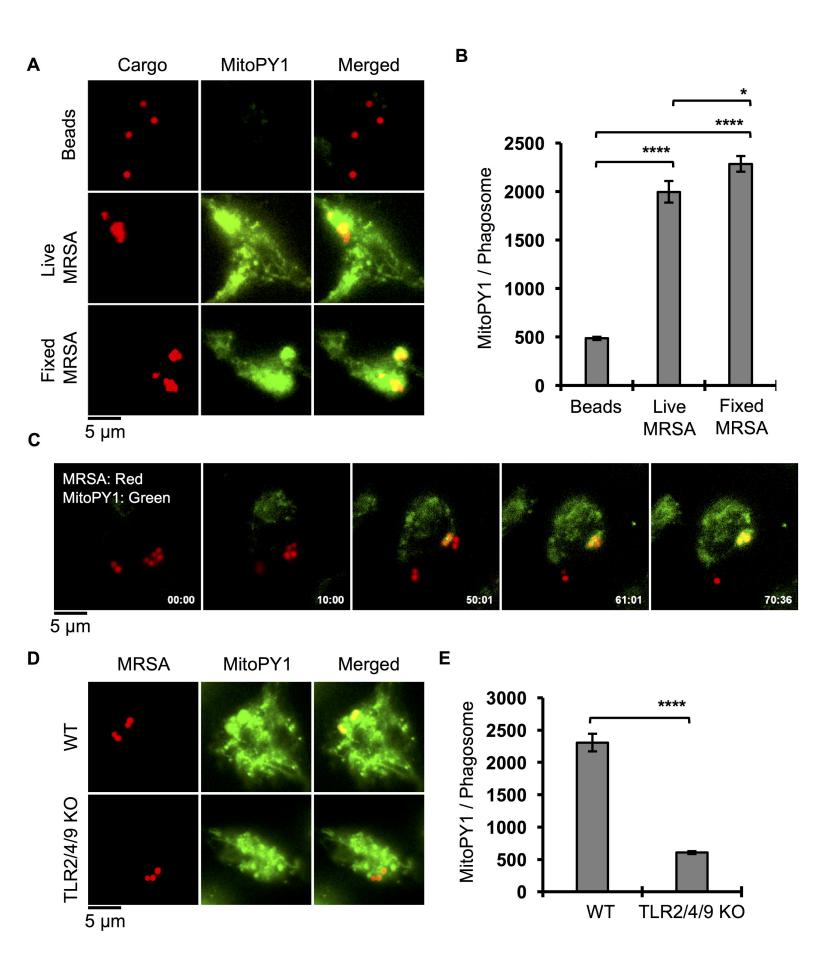
871 Movie S1. mH₂O₂ accumulates in MRSA-containing phagosome

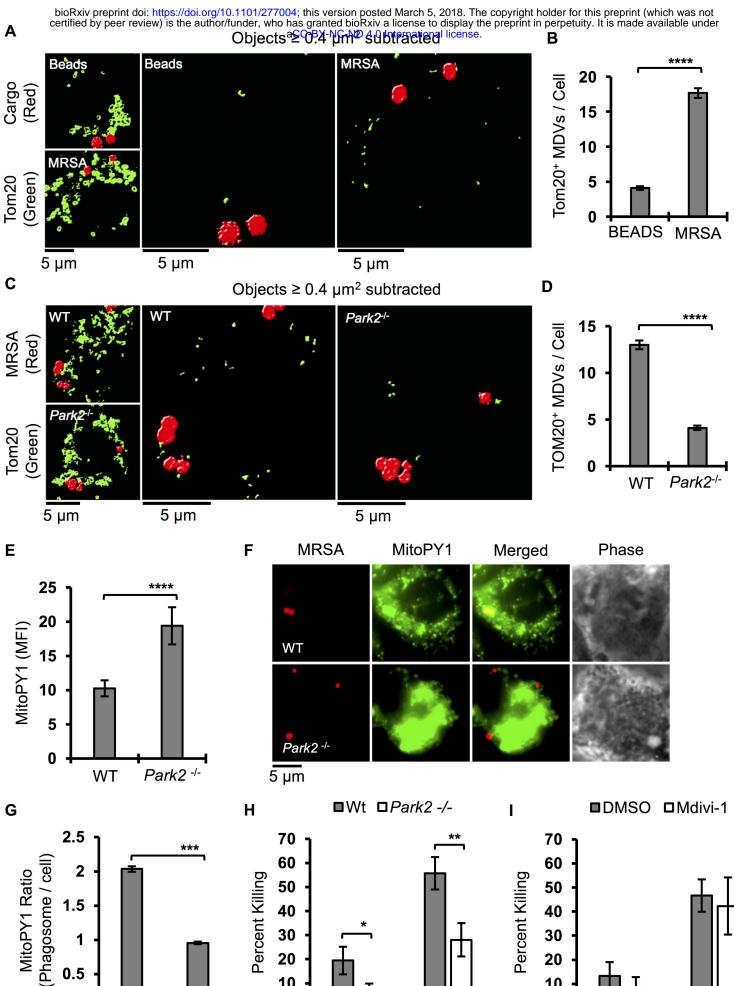
Time-lapse movie of RAW264.7 macrophage after being pulsed with mitochondriatargeted H₂O₂ fluorescent sensor, MitoPY1 (green fluorescent) for 1h and infected with MRSA-mCherry (Red fluorescent). Images were acquired using inverted IX-70 Olympus

875 live fluorescent microscope and analyzed using MetaMorph imaging software. Time

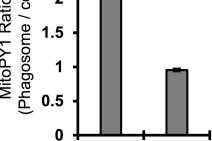
876 clock Minutes : Seconds.





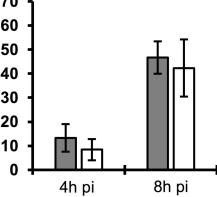


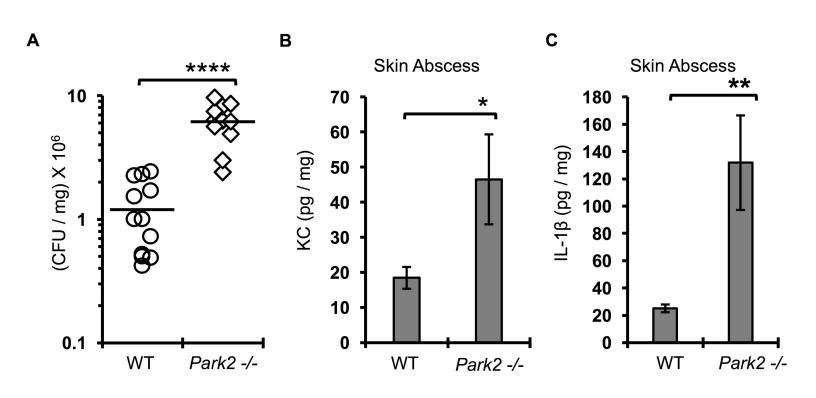
8h pi

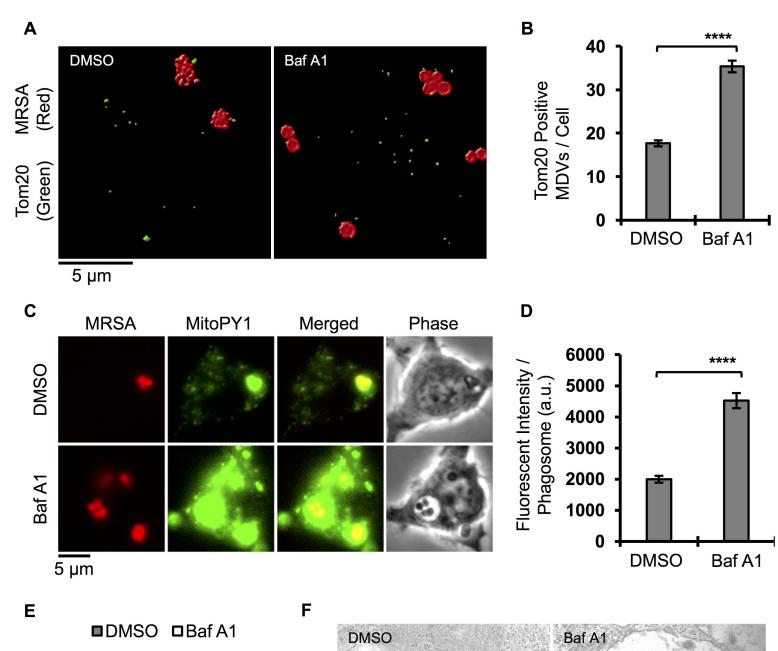


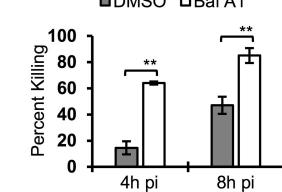
WT

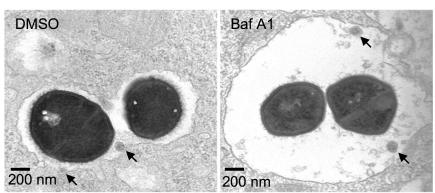
10 0 Park2 -/-4h pi

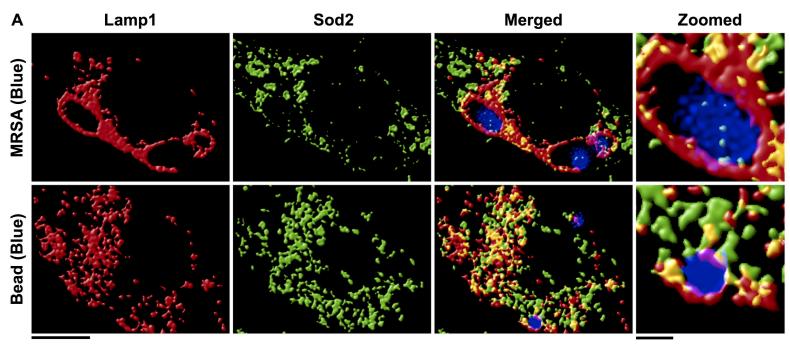






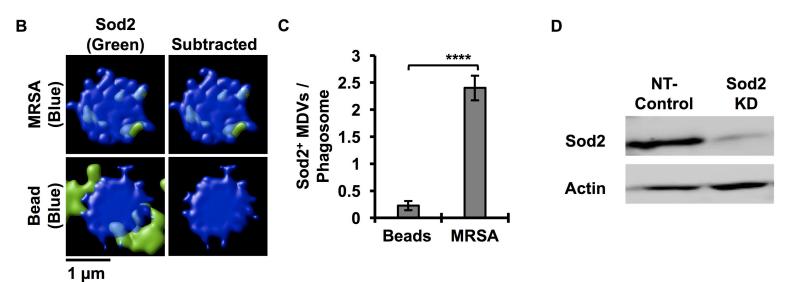






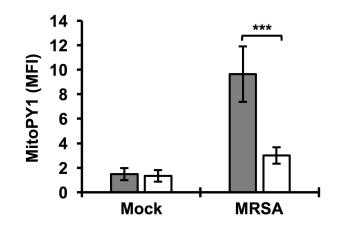
5 µm

1 µm



Е





F

